

Mars's Moons-Induced Time Dispersion Analysis for Solar TDOA Navigation

Yang-yang Li¹, Jin Liu¹ , Xiao-lin Ning² , Xiao Chen³ and Zhi-wei Kang⁴

¹(College of Information Science and Engineering, Wuhan University of Science and Technology, Wuhan 430081, People's Republic of China)

²(School of Instrumentation Science & Opto-electronics Engineering, Beihang University (BUAA), Beijing 100191, People's Republic of China)

³(Shanghai Institution of Satellite Engineering, Shanghai 200240, People's Republic of China)

⁴(College of Computer Science and Electronic Engineering, Hunan University, Changsha 410082, People's Republic of China)
(E-mail: liujin@wust.edu.cn)

The time dispersion effect affects the accuracy of solar time difference of arrival (TDOA) navigation. In this celestial autonomous navigation, Mars's moons are reflecting celestial bodies, and their shape affects the TDOA dispersion model. In the modelling process of traditional methods, the moons of Mars (Phobos and Deimos) are regarded as points, which causes the model to be inaccurate. In order to solve these problems, we simplified the Mars's moons into ellipsoids or solid diamonds, and then established a TDOA model with the nonspherical Mars's moons as reflecting celestial bodies through differential geometry and geometric optics. Finally, we analysed the time dispersion caused by the Mars's moons in theory. Theoretical analysis and experiments show that the point model error is 5.66 km, and the 3D model error is within 70 m. Thus, the 3D TDOA model established in this paper is meaningful. In addition, the Sun–Mars–moons–spacecraft angle, solar flare, three-axis length, and attitude of the Mars's moons have a great effect on the dispersion profile, while the Mars's moons-to-spacecraft distance has a small effect.

KEY WORDS

1. Time Dispersion. 2. TDOA. 3. Mars. 4. Modelling. 5. Navigation.

Submitted: 25 May 2020. Accepted: 13 August 2020. First published online: 15 September 2020.

1. INTRODUCTION. Celestial navigation uses the optical signals emitted or reflected by celestial bodies to calculate the carrier position (Li et al., 2006; Wang et al., 2007). The stars (Sun) radiate external signals, and celestial bodies such as asteroids reflect the optical signals from the stars. Deep-space explorers can achieve real-time celestial navigation by receiving these signals and processing them (Fang et al., 2017). Because they are not limited by ground stations, the celestial autonomous navigation methods are particularly

important in the approach phase of deep space exploration (Yan et al., 2016). Traditional celestial autonomous navigation methods include angle measurement (Konopliv et al., 2011; Yu et al., 2014; Wang et al., 2017), speed measurement (Long et al., 2000; Chen et al., 2019; Christian, 2019), and distance measurement (Sheikh et al., 2006; Liu et al., 2015a; Sun et al., 2016; Zhang et al., 2019). But these methods fail to provide the radial navigation information (such as distance and velocity) between the spacecraft and the target celestial body in the approach phase of deep space exploration. To solve this problem, the direct light of the Sun and the reflected light of the planet are compared to obtain the distance and velocity information of the spacecraft relative to the target celestial body. In 2015, Liu proposed a solar Doppler velocity difference method (Liu et al., 2015b). Subsequently, many scientific research institutes also carried out research in this field and achieved a series of results. Ning proposed a novel differential Doppler measurement that aided celestial navigation method for spacecraft during the approach phase (Ning et al., 2018b). Kang proposed a Doppler velocity measurement based on the double measurement model and its integrated navigation (Kang et al., 2017). Pantalone and Cedeno used Doppler frequency shifting of the Fraunhofer lines for celestial navigation (Pantalone and Kudenov, 2018). In 2017, inspired by the idea of Doppler velocity difference, Liu developed the solar time difference of arrival (TDOA) navigation method (Liu et al., 2017b). The solar TDOA navigation uses light-intensity meters to receive photons directly emitted from the Sun and solar photons reflected by Mars, and measures the arrival time of the two respectively. The difference between them can reflect the radial distance information. Ning also carried out related research in this field, and proposed a solar oscillation time-delay measurement-assisted celestial navigation method (Ning et al., 2017; Ning et al., 2018a). In addition, these methods can also be used for relative navigation (Liu et al., 2017a; Wang et al., 2020; Yu et al., 2019). In summary, solar difference navigation has become a research hotspot.

In the solar difference navigation, the establishment of measurement models is an important work (Liu et al., 2020). In 2017, in the original of the solar TDOA navigation concept proposed by Liu, the shapes of the Sun and Mars were ignored. Under these conditions, a TDOA measurement model was constructed. However, the time difference of arrival at different locations at the solar surface is different. And the shape of the Sun has an impact on the TDOA measurement model. In response to this problem, two years later, Liu approximated the Mars's moons (Phobos and Deimos) to a point, and treated the Sun as a huge sphere. Under these conditions, Liu established a time dispersion model caused by the solar sphere, and the error analysis of the solar TDOA navigation was carried out (Liu et al., 2019).

However, this is not the reality, and the shape of the Mars's moons are not points. In fact, the shapes of the Mars's moons cannot be ignored, nor can they be regarded as spherical. Their shapes affect the measurement of the solar TDOA and the accuracy of the solar TDOA navigation. In this paper, starting from the basic principle of the measurement method of the solar TDOA, the solar TDOA measurement model proposed in Ref (Liu et al., 2019) is modified by differential geometry and geometric optics. The shapes of Mars's moons are fitted as accurately as possible. The solar TDOA measurement model based on the nonspherical Mars's moons is developed. And the time dispersion caused by the nonspherical Mars's moons for the solar TDOA navigation is analysed. To improve navigation performance, this analysis can be used to compensate for errors.

This article is divided into six parts. After the introduction, we present the coordinate system used in this article in Section 2. In Section 3, we present the measurement model

of the solar TDOA and the basic principles of time dispersion caused by non-spherical the Mars's moons. Section 4 analyses and proves the properties of the time dispersion model caused by the nonspherical Mars's moons. Section 5 shows the corresponding simulation results and analysis, and finally draws conclusions.

2. CALCULATION COORDINATE SYSTEM. To facilitate navigation calculation, the calculation coordinate system is established as shown in Figure 1. The Mars's moons are ellipsoids, and the origin of the calculated coordinate system is the Mars's moons centroid. The solar centroid is on the z -axis, and the spacecraft is on the y - z plane. The x -axis is perpendicular to the y - z plane and forms a right-handed coordinate system with it.

Using the space rectangular coordinate system established in Figure 1, the parametric equations of the Mars's moons are shown as

$$\begin{cases} x = a \sin \varphi \cos \theta \\ y = b \sin \varphi \sin \theta (0 \leq \varphi \leq \pi, 0 \leq \theta < 2\pi) \\ z = c \cos \varphi \end{cases} \quad (1)$$

Since the Mars's moons are ellipsoids, the three semi-axes are defined as a , b , and c , and their values are 13.5 km, 10.7 km and 9.6 km, respectively.

As shown in Figure 2, c is used as the radius to make the spherical surface. Passing arbitrary point P at the surface of the ellipsoid makes the plane β perpendicular to the z -axis. The plane β has a line of intersection with the spherical surface. Take O as the vertex and the intersection line as the base circle to form a cone. The angle between the conical generatrix and the z -axis is φ .

As shown in Figure 3, we use O as the centre of the circle, and draw circles a and b , respectively. The point B is the intersection of the large circle radius surface OM and the small circle. Making MN perpendicular to OX , the pedal is N . And making BP perpendicular to MN , the pedal is P . Then the locus of point P is the ellipsoid section, and $\angle XOM$ is θ .

3. BASIC PRINCIPLE OF TIME DISPERSION. In this section, we establish a 3D model with the Mars's moons considered as ellipsoids. And we introduce the basic principle of Mars's moons-induced time dispersion for the solar TDOA navigation.

The Mars's moons are not the points, but the ellipsoids. For different points at the surface of the Mars's moons, the solar TDOAs are different, which leads to the time dispersion caused by the Mars's moons for the solar TDOA navigation. Using the coordinate system established in the Section 2, the basic principle is shown in Figure 4. Assume that the starting point of both direct sunlight and reflected light is the centre of the Sun. Point P is the reflected point at the surface of the Mars's moons. Points S and E represent the solar centroid and the spacecraft, respectively.

Then we derive the expression of the solar TDOA relative to the reflection point. Suppose two solar photons leave point S at time t_0 . A solar photon flies directly to the spacecraft, which is captured at point E at time t_1 . The other is reflected by the Mars's moons (point P) at time t_p and captured at point E at time t . The difference between time t and t_1 is the solar TDOA.

The sunlight comes from the centre of the Sun (point S). Assume that the solar photons pass through the Mars's moons and reach the centroid O of Mars's moons. The direct

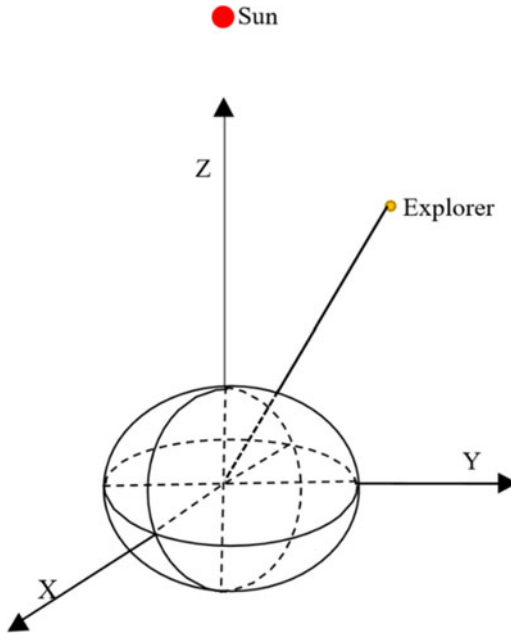


Figure 1. Space rectangular coordinate system.

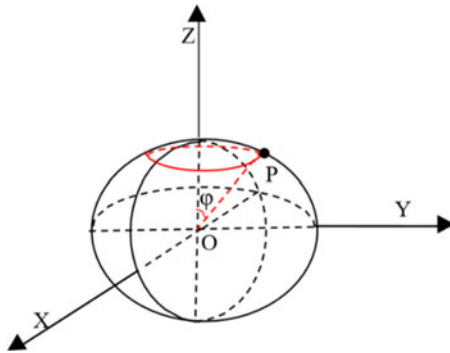


Figure 2. Ellipsoid.

flight distance of the solar photon is $|ES|$, and the corresponding flight time is $t_1 - t_0$. The reflected flight distance of the solar photon is $|OS| + |EO|$, and the corresponding flight time is $(t_P - t_0) + (t - t_0)$. The ideal TDOA is shown as

$$\begin{aligned}
 c(t - t_1) &= c(t_P - t_0) + c(t - t_P) - c(t_1 - t_0) \\
 &= |SO| + |EO| - |ES| \\
 &= z_s + \sqrt{y_e^2 + z_e^2} - \sqrt{y_e^2 + (z_e - z_s)^2}
 \end{aligned}
 \tag{2}$$

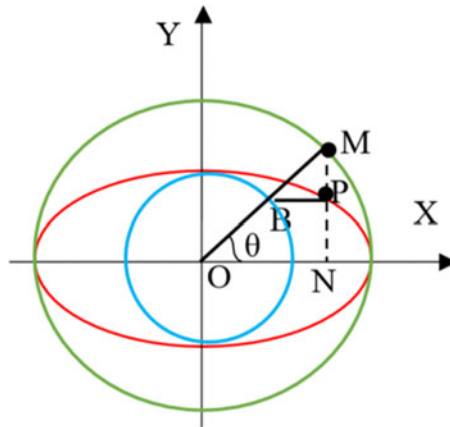


Figure 3. Ellipsoid section.

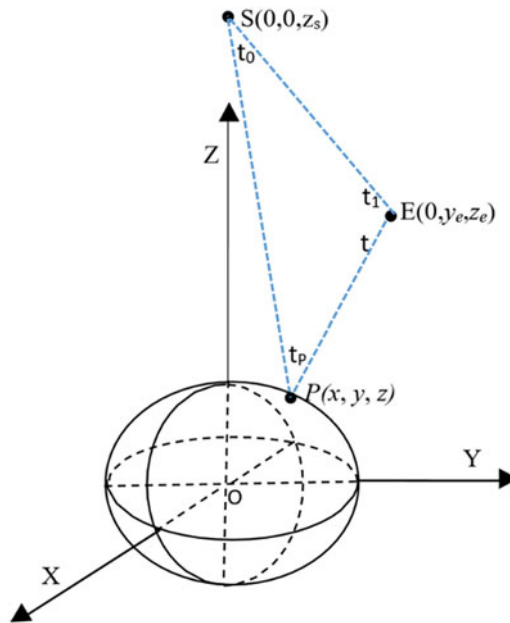


Figure 4. Principle of time dispersion.

In fact, the reflection of sunlight is at the surface of the Mars’s moons, not in the centre of the Mars’s moons. More precisely, the actual TDOA is shown as

$$\begin{aligned}
 c(t - t_1) &= c(t_p - t_0) + c(t - t_p) - c(t_1 - t_0) = |SP| + |EP| - |ES| \\
 &= \sqrt{x^2 + y^2 + (z - z_s)^2} + \sqrt{x^2 + (y - y_e)^2 + (z - z_e)^2} - \sqrt{y_e^2 + (z_e - z_s)^2} \\
 &= \sqrt{x^2 + y^2 + z^2 + z_s^2 - 2zz_s} + \sqrt{x^2 + y^2 + y_e^2 + z^2 + z_e^2 - 2yy_e - 2zz_e} \\
 &\quad - \sqrt{y_e^2 + z_e^2 + z_s^2 - 2z_s z_e}
 \end{aligned} \tag{3}$$

$$S_2 = \{P | \angle POE \leq T_2OE\} \tag{7}$$

$$S_{12} = \{P | \angle POS \leq T_2OS = \theta_1, \angle POE \leq T_2OE\} \tag{8}$$

In Equation (8) can be rewritten as

$$0 < \theta < \theta_1 \tag{9}$$

$$\angle EPO > \frac{\pi}{2} \tag{10}$$

We define $\angle EPO$ as θ_2 . In Equation (10) can be rewritten as

$$\theta_2 = a \cos \frac{\left(\sqrt{x^2 + (y - y_e)^2 + (z - z_e)^2}\right)^2 + \left(\sqrt{x^2 + y^2 + z^2}\right)^2 - \left(\sqrt{y_e^2 + z_e^2}\right)^2}{2\sqrt{x^2 + (y - y_e)^2 + (z - z_e)^2}\sqrt{x^2 + y^2 + z^2}} > \frac{\pi}{2} \tag{11}$$

According to In Equations (9) and (11), the coincident area, S_{12} , can be presented as

$$S_{12} = S_1 \cap S_2 = \left\{ P \mid 0 \leq \varphi \leq 2\pi, 0 \leq \theta \leq \theta_1, \theta_2 \geq \frac{\pi}{2} \right\} \tag{12}$$

where r_{SMn} = Sun-to-Mars’s moons distance, θ_1 = angle of the Sun directly on the Mars’s moons, S_1 = area where Mars’s moons can be irradiated by the Sun, θ_2 = angle at which Mars’s moons can reflect on the spacecraft, S_2 = area where Mars’s moons can reflect on the spacecraft, and S_{12} = coincident area.

In summary, we can combine Equations (1), (3) and (9) to calculate the TDOA in this coincident area and analyse the time dispersion caused by the Mars’s moons for the solar TDOA navigation. In practical application, both the direct light and the reflected light are received by the spacecraft. According to the probability distribution of time dispersion, the direct light is processed by delay and expansion to simulate the reflected light. Then, the reflected light and the simulated light are cross-correlated to provide the velocity information.

4. THEORETICAL ANALYSIS. In this section, we theoretically analyse two faces, including the shapes of the Mars’s moons and the Mars’s moons-to-spacecraft distance. The shapes of the Mars’s moons on the time dispersion are given as Theorem 1. The relationship between the time dispersion caused by the Mars’s moons and the Mars’s moons-to-spacecraft distance given as Theorem 2. Proofs are given respectively.

THEOREM 1: *The time dispersion caused by the Mars’s moons is uncorrelated to the position of the starting point at the solar surface.*

Proof. Assume that there are two points $M(x_{s1}, y_{s1}, z_{s1})$ and $N(x_{s2}, y_{s2}, z_{s2})$ at the solar surface. The two points $A(x_1, y_1, z_1)$ and $B(x_2, y_2, z_2)$ are at the surface of the Mars’s moons, and the coordinates of the spacecraft is $E(x_e, y_e, z_e)$. We define the time dispersion width as the difference between the maximum value and the minimum value of the TDOA.

The principle of the time dispersion is shown in Section 3. The time dispersion width T_W of the two points on the Sun can be expressed as

$$\begin{aligned}
 T_{WM} &= \frac{1}{C} \left(\begin{array}{c} \left(\begin{array}{c} \sqrt{(x_1 - x_{s1})^2 + (y_1 - y_{s1})^2 + (z_1 - z_{s1})^2} \\ +\sqrt{(x_1 - x_e)^2 + (y_1 - y_e)^2 + (z_1 - z_e)^2} \\ -\sqrt{(x_e - x_{s1})^2 + (y_e - y_{s1})^2 + (z_e - z_{s1})^2} \end{array} \right) \\ - \left(\begin{array}{c} \sqrt{(x_2 - x_{s1})^2 + (y_2 - y_{s1})^2 + (z_2 - z_{s1})^2} \\ +\sqrt{(x_2 - x_e)^2 + (y_2 - y_e)^2 + (z_2 - z_e)^2} \\ -\sqrt{(x_e - x_{s1})^2 + (y_e - y_{s1})^2 + (z_e - z_{s1})^2} \end{array} \right) \end{array} \right) \\
 &= \frac{1}{C} \left(\begin{array}{c} \sqrt{(x_1 - x_{s1})^2 + (y_1 - y_{s1})^2 + (z_1 - z_{s1})^2} \\ +\sqrt{(x_1 - x_e)^2 + (y_1 - y_e)^2 + (z_1 - z_e)^2} \\ -\sqrt{(x_2 - x_{s1})^2 + (y_2 - y_{s1})^2 + (z_2 - z_{s1})^2} \\ -\sqrt{(x_2 - x_e)^2 + (y_2 - y_e)^2 + (z_2 - z_e)^2} \end{array} \right) \tag{13}
 \end{aligned}$$

$$\begin{aligned}
 T_{WN} &= \frac{1}{C} \left(\begin{array}{c} \left(\begin{array}{c} \sqrt{(x_1 - x_{s2})^2 + (y_1 - y_{s2})^2 + (z_1 - z_{s2})^2} \\ +\sqrt{(x_1 - x_e)^2 + (y_1 - y_e)^2 + (z_1 - z_e)^2} \\ -\sqrt{(x_e - x_{s2})^2 + (y_e - y_{s2})^2 + (z_e - z_{s2})^2} \end{array} \right) \\ - \left(\begin{array}{c} \sqrt{(x_2 - x_{s2})^2 + (y_2 - y_{s2})^2 + (z_2 - z_{s2})^2} \\ +\sqrt{(x_2 - x_e)^2 + (y_2 - y_e)^2 + (z_2 - z_e)^2} \\ -\sqrt{(x_e - x_{s2})^2 + (y_e - y_{s2})^2 + (z_e - z_{s2})^2} \end{array} \right) \end{array} \right) \\
 &= \frac{1}{C} \left(\begin{array}{c} \sqrt{(x_1 - x_{s2})^2 + (y_1 - y_{s2})^2 + (z_1 - z_{s2})^2} \\ +\sqrt{(x_1 - x_e)^2 + (y_1 - y_e)^2 + (z_1 - z_e)^2} \\ -\sqrt{(x_2 - x_{s2})^2 + (y_2 - y_{s2})^2 + (z_2 - z_{s2})^2} \\ -\sqrt{(x_2 - x_e)^2 + (y_2 - y_e)^2 + (z_2 - z_e)^2} \end{array} \right) \tag{14}
 \end{aligned}$$

The difference in time dispersion width between the two points of the Sun is expressed by ΔT_{W-MN} as

$$\begin{aligned}
 \Delta T_{W-MN} &= T_{WM} - T_{WN} \\
 &= \frac{1}{C} \left(\begin{array}{c} \sqrt{(x_1 - x_{s1})^2 + (y_1 - y_{s1})^2 + (z_1 - z_{s1})^2} \\ +\sqrt{(x_1 - x_e)^2 + (y_1 - y_e)^2 + (z_1 - z_e)^2} \\ -\sqrt{(x_2 - x_{s1})^2 + (y_2 - y_{s1})^2 + (z_2 - z_{s1})^2} \\ -\sqrt{(x_2 - x_e)^2 + (y_2 - y_e)^2 + (z_2 - z_e)^2} \end{array} \right)
 \end{aligned}$$

$$\begin{aligned}
 & -\frac{1}{C} \left(\begin{array}{c} \sqrt{(x_1 - x_{s2})^2 + (y_1 - y_{s2})^2 + (z_1 - z_{s2})^2} \\ +\sqrt{(x_1 - x_e)^2 + (y_1 - y_e)^2 + (z_1 - z_e)^2} \\ -\sqrt{(x_2 - x_{s2})^2 + (y_2 - y_{s2})^2 + (z_2 - z_{s2})^2} \\ -\sqrt{(x_2 - x_e)^2 + (y_2 - y_e)^2 + (z_2 - z_e)^2} \end{array} \right) \\
 & = \frac{1}{C} \left(\begin{array}{c} \sqrt{(x_1 - x_{s1})^2 + (y_1 - y_{s1})^2 + (z_1 - z_{s1})^2} \\ -\sqrt{(x_2 - x_{s1})^2 + (y_2 - y_{s1})^2 + (z_2 - z_{s1})^2} \\ +\sqrt{(x_2 - x_{s2})^2 + (y_2 - y_{s2})^2 + (z_2 - z_{s2})^2} \\ -\sqrt{(x_1 - x_{s2})^2 + (y_1 - y_{s2})^2 + (z_1 - z_{s2})^2} \end{array} \right) \\
 & = \frac{1}{C} \left(\begin{array}{c} \frac{x_1^2 - 2x_1x_{s1} + y_1^2 - 2y_1y_{s1} + z_1^2 - 2z_1z_{s1} - x_2^2 + 2x_2x_{s1} - y_2^2 + 2y_2y_{s1} - z_2^2 + 2z_2z_{s1}}{\sqrt{(x_1 - x_{s1})^2 + (y_1 - y_{s1})^2 + (z_1 - z_{s1})^2} + \sqrt{(x_2 - x_{s1})^2 + (y_2 - y_{s1})^2 + (z_2 - z_{s1})^2}} \\ + \frac{x_2^2 - 2x_2x_{s2} + y_2^2 - 2y_2y_{s2} + z_2^2 - 2z_2z_{s2} - x_1^2 + 2x_1x_{s2} - y_1^2 + 2y_1y_{s2} - z_1^2 + 2z_1z_{s2}}{\sqrt{(x_2 - x_{s2})^2 + (y_2 - y_{s2})^2 + (z_2 - z_{s2})^2} + \sqrt{(x_1 - x_{s2})^2 + (y_1 - y_{s2})^2 + (z_1 - z_{s2})^2}} \end{array} \right) \\
 & \approx \frac{2}{C} \frac{(x_1 - x_2)(x_{s2} - x_{s1}) + (y_1 - y_2)(y_{s2} - y_{s1}) + (z_1 - z_2)(z_{s2} - z_{s1})}{\sqrt{(x_1 - x_{s1})^2 + (y_1 - y_{s1})^2 + (z_1 - z_{s1})^2}} \\
 & \approx 0 \tag{15}
 \end{aligned}$$

From these equations, we can see that the time dispersion width difference between two points at the solar surface is almost unchanged, which indicates that the time dispersion profile of any point at the solar surface is almost the same. And the time dispersion width of any point at the solar surface is also constant. Analysing Equation (15), we calculate that the magnitude of the error is about 10^{-8} s.

The time dispersion at a point on the Sun is defined as the difference between the maximum and minimum values of the TDOA:

$$T_W = \frac{1}{C} \left(\begin{array}{c} \sqrt{x_1^2 + y_1^2 + (z_1 - z_s)^2} + \sqrt{x_1^2 + (y_1 - y_e)^2 + (z_1 - z_e)^2} \\ -\sqrt{x_2^2 + y_2^2 + (z_2 - z_s)^2} - \sqrt{x_2^2 + (y_2 - y_e)^2 + (z_2 - z_e)^2} \end{array} \right) \tag{16}$$

where the solar coordinate is $(0, 0, z_s)$, and the coordinates of the spacecraft is $(0, y_e, z_e)$.

Assume f is the component of T_W , it can be expressed as

$$f = \sqrt{x^2 + y^2 + (z - z_s)^2} + \sqrt{x^2 + (y - y_e)^2 + (z - z_e)^2} \tag{17}$$

Finding the maximum and minimum values of f respectively, we can find the time dispersion of a point on the Sun. Taking Equation (1) into f , we get

$$\begin{aligned}
 f & = \sqrt{x^2 + y^2 + (z - z_s)^2} + \sqrt{x^2 + (y - y_e)^2 + (z - z_e)^2} \\
 & = \sqrt{(a \sin \theta \cos \varphi)^2 + (b \sin \theta \sin \varphi)^2 + (c \cos \theta - z_s)^2} \\
 & \quad + \sqrt{(a \sin \theta \cos \varphi)^2 + (b \sin \theta \sin \varphi - y_e)^2 + (c \cos \theta - z_e)^2} \tag{18}
 \end{aligned}$$

Taking partial derivatives for f , we get

$$\left\{ \begin{aligned} f_\theta &= \frac{a^2 \sin \theta \cos \theta \cos^2 \varphi + b^2 \sin \theta \cos \theta \sin^2 \varphi - (c \cos \theta - z_s) c \sin \theta}{\sqrt{(a \sin \theta \cos \varphi)^2 + (b \sin \theta \sin \varphi)^2 + (c \cos \theta - z_s)^2}} \\ &+ \frac{a^2 \sin \theta \cos \theta \cos^2 \varphi + (b \sin \theta \sin \varphi - y_e) b \cos \theta \sin \varphi - (c \cos \theta - z_s) c \sin \theta}{\sqrt{(a \sin \theta \cos \varphi)^2 + (b \sin \theta \sin \varphi - y_e)^2 + (c \cos \theta - z_e)^2}} = 0 \\ f_\varphi &= \frac{-a^2 \sin^2 \theta \sin \varphi \cos \varphi + b^2 \sin^2 \theta \sin \varphi \cos \varphi}{\sqrt{(a \sin \theta \cos \varphi)^2 + (b \sin \theta \sin \varphi)^2 + (c \cos \theta - z_s)^2}} \\ &+ \frac{-a^2 \sin^2 \theta \sin \varphi \cos \varphi + (b \sin \theta \sin \varphi - y_e) b \sin \theta \cos \varphi}{\sqrt{(a \sin \theta \cos \varphi)^2 + (b \sin \theta \sin \varphi - y_e)^2 + (c \cos \theta - z_e)^2}} = 0 \end{aligned} \right. \tag{19}$$

We can obtain the solutions as

$$\begin{cases} \theta = 0 \\ \varphi = 0 \end{cases} \tag{20}$$

$$\begin{cases} \tan \theta = \frac{by_e}{c(z_e + \sqrt{y_e^2 + z_e^2})} \\ \varphi = \frac{\pi}{2} \end{cases} \tag{21}$$

Considering the boundary points of the ellipsoid, the maximum and minimum points are finally obtained as

$$\begin{cases} \theta = \frac{\pi}{2} \\ \varphi = 0 \end{cases} \tag{22}$$

$$\begin{cases} \tan \theta = \frac{by_e}{c(z_e + \sqrt{y_e^2 + z_e^2})} \approx \frac{b}{4c} \\ \varphi = \frac{\pi}{2} \end{cases} \tag{23}$$

By taking Equation (22) and Equation (23) into Equation (18), the maximum and minimum values of f can be obtained as

$$f_{Max} = \sqrt{a^2 + 0^2 + (0 - z_s)^2} + \sqrt{a^2 + (0 - y_e)^2 + (0 - z_e)^2} = \sqrt{a^2 + z_s^2} + \sqrt{a^2 + y_e^2 + z_e^2} \tag{24}$$

$$\begin{aligned} f_{Min} &= \sqrt{\left(b \sin \left(\text{actan} \frac{b}{4c}\right)\right)^2 + \left(c \cos \left(\text{actan} \frac{b}{4c}\right) - z_s\right)^2} \\ &+ \sqrt{\left(b \sin \left(\text{actan} \frac{b}{4c}\right) - y_e\right)^2 + \left(c \cos \left(\text{actan} \frac{b}{4c}\right) - z_e\right)^2} \end{aligned} \tag{25}$$

The time dispersion width T_W can then be expressed as

$$T_W = f_{\text{Max}} - f_{\text{Min}} = \frac{1}{C} \left(\begin{array}{l} \sqrt{a^2 + z_s^2} + \sqrt{a^2 + y_e^2 + z_e^2} \\ -\sqrt{(b \sin(\text{actan} \frac{b}{4c}))^2 + (c \cos(\text{actan} \frac{b}{4c}) - z_s)^2} \\ -\sqrt{(b \sin(\text{actan} \frac{b}{4c}) - y_e)^2 + (c \cos(\text{actan} \frac{b}{4c}) - z_e)^2} \end{array} \right) \quad (26)$$

It can be seen from this equation that the value in the time dispersion width T_W expression is unchanged, that is, the time dispersion at any point on the Sun is constant. The time dispersion width of the point at the solar surface is given as follows.

For the convenience of analysis, Equation (26) can be simplified as

$$\begin{aligned} T_W &= \frac{1}{C} \left(\begin{array}{l} \sqrt{a^2 + z_s^2} - \sqrt{(b \sin(\text{actan} \frac{b}{4c}))^2 + (c \cos(\text{actan} \frac{b}{4c}) - z_s)^2} \\ +\sqrt{a^2 + y_e^2 + z_e^2} - \sqrt{(b \sin(\text{actan} \frac{b}{4c}) - y_e)^2 + (c \cos(\text{actan} \frac{b}{4c}) - z_e)^2} \end{array} \right) \\ &= \frac{1}{C} \left(\begin{array}{l} z_s \sqrt{1 + \frac{a^2}{z_s^2}} - z_s \sqrt{\frac{(b \sin(\text{actan} \frac{b}{4c}))^2}{z_s^2} + 1 - \frac{2c \cos(\text{actan} \frac{b}{4c})}{z_s} + \frac{(c \cos(\text{actan} \frac{b}{4c}))^2}{z_s^2}} \\ +z_e \sqrt{\frac{a^2}{z_e^2} + \frac{y_e^2}{z_e^2} + 1} - z_e \sqrt{\frac{(b \sin(\text{actan} \frac{b}{4c}))^2}{z_e^2} - \frac{2y_e b \sin(\text{actan} \frac{b}{4c})}{z_e^2} + \frac{y_e^2}{z_e^2} + \frac{(c \cos(\text{actan} \frac{b}{4c}))^2}{z_e^2} - \frac{2c \cos(\text{actan} \frac{b}{4c})}{z_e} + 1} \end{array} \right) \\ &\approx \frac{1}{C} \left(\begin{array}{l} z_s \left(\left(1 + \frac{1}{2} \frac{a^2}{z_s^2} \right) - \left(1 + \frac{1}{2} \frac{(b \sin(\text{actan} \frac{b}{4c}))^2}{z_s^2} - \frac{c \cos(\text{actan} \frac{b}{4c})}{z_s} + \frac{1}{2} \frac{(c \cos(\text{actan} \frac{b}{4c}))^2}{z_s^2} \right) \right) \\ +z_e \left(\left(1 + \frac{1}{2} \frac{a^2}{z_e^2} + \frac{1}{2} \frac{y_e^2}{z_e^2} \right) - \left(1 + \frac{1}{2} \frac{(b \sin(\text{actan} \frac{b}{4c}))^2}{z_e^2} - \frac{y_e b \sin(\text{actan} \frac{b}{4c})}{z_e^2} + \frac{1}{2} \frac{y_e^2}{z_e^2} + \frac{1}{2} \frac{(c \cos(\text{actan} \frac{b}{4c}))^2}{z_e^2} - \frac{c \cos(\text{actan} \frac{b}{4c})}{z_e} \right) \right) \end{array} \right) \\ &= \frac{1}{C} \left(\begin{array}{l} 2c \cos(\text{actan} \frac{b}{4c}) + \frac{y_e b \sin(\text{actan} \frac{b}{4c})}{z_e} \\ +z_s \left(\frac{1}{2} \frac{a^2 - (b \sin(\text{actan} \frac{b}{4c}))^2 - (c \cos(\text{actan} \frac{b}{4c}))^2}{z_s^2} \right) \\ +z_e \left(\frac{1}{2} \frac{a^2 - (b \sin(\text{actan} \frac{b}{4c}))^2 - (c \cos(\text{actan} \frac{b}{4c}))^2}{z_e^2} \right) \end{array} \right) \quad (27) \end{aligned}$$

During the approach phase, the magnitude of z_s is approximately on the order of 10^8 km, the magnitude of z_e is approximately 10^6 km, and the magnitude of C is 10^5 km/s. So, the estimated the magnitude of time dispersion T_W is approximately 10^{-5} s.

In summary, the time dispersion caused by the Mars’s moons is uncorrelated to the position of the starting point at the solar surface.

This completes the proof of Theorem 1. ■

THEOREM 2: *The time dispersion width is unrelated to the Mars’s moons-to-spacecraft distance.*

Proof. Let r_{EMn} be the Mars’s moons-to-spacecraft distance. During the approach of the spacecraft to the Mars’s moons, the Mars’s moons-to-spacecraft distance r_{EMn} is constantly changing. With r_{EMn} as a variable, the time dispersion width is analysed.

The time dispersion is shown in Section 3. Taking the Mars's moons-to-spacecraft distance r_{EMn} as a variable, the time dispersion, Equation (4) can be expressed as

$$\begin{aligned}
 T_W &= \frac{1}{C} \left(\begin{aligned} &\left(\sqrt{x_1^2 + y_1^2 + (z_1 - z_s)^2} + \sqrt{x_1^2 + (y_1 - y_e)^2 + (z_1 - z_e)^2} \right) \\ &- \sqrt{x_e^2 + y_e^2 + (z_e - z_s)^2} \\ &- \left(\sqrt{x_2^2 + y_2^2 + (z_2 - z_s)^2} + \sqrt{x_2^2 + (y_2 - y_e)^2 + (z_2 - z_e)^2} \right) \\ &- \sqrt{x_e^2 + y_e^2 + (z_e - z_s)^2} \end{aligned} \right) \\
 &= \frac{1}{C} \left(\begin{aligned} &\left(\sqrt{x_1^2 + y_1^2 + (z_1 - z_s)^2} + \sqrt{x_1^2 + (y_1 - y_e)^2 + (z_1 - z_e)^2} \right) \\ &- \sqrt{x_2^2 + y_2^2 + (z_2 - z_s)^2} - \sqrt{x_2^2 + (y_2 - y_e)^2 + (z_2 - z_e)^2} \end{aligned} \right) \\
 &= \frac{1}{C} \left(\begin{aligned} &\left(\sqrt{x_1^2 + y_1^2 + (z_1 - r_{SMn})^2} + \sqrt{x_1^2 + (y_1 - r_{EMn} \sin \alpha)^2 + (z_1 - r_{EMn} \cos \alpha)^2} \right) \\ &- \sqrt{x_2^2 + y_2^2 + (z_2 - r_{SMn})^2} - \sqrt{x_2^2 + (y_2 - r_{EMn} \sin \alpha)^2 + (z_2 - r_{EMn} \cos \alpha)^2} \end{aligned} \right) \\
 &= \frac{1}{C} \left(\begin{aligned} &\left(\frac{x_1^2 + y_1^2 + (z_1 - r_{SMn})^2 - x_2^2 - y_2^2 - (z_2 - r_{SMn})^2}{\sqrt{x_1^2 + y_1^2 + (z_1 - r_{SMn})^2} + \sqrt{x_2^2 + y_2^2 + (z_2 - r_{SMn})^2}} \right. \\ &\left. + \frac{x_1^2 + (y_1 - r_{EMn} \sin \alpha)^2 + (z_1 - r_{EMn} \cos \alpha)^2 - x_2^2 - (y_2 - r_{EMn} \sin \alpha)^2 - (z_2 - r_{EMn} \cos \alpha)^2}{\sqrt{x_1^2 + (y_1 - r_{EMn} \sin \alpha)^2 + (z_1 - r_{EMn} \cos \alpha)^2} + \sqrt{x_2^2 + (y_2 - r_{EMn} \sin \alpha)^2 + (z_2 - r_{EMn} \cos \alpha)^2}} \right) \\
 &\approx \frac{1}{C} \left(\begin{aligned} &\left(\frac{2(z_2 - z_1)r_{SMn}}{\sqrt{x_1^2 + y_1^2 + (z_1 - r_{SMn})^2} + \sqrt{x_2^2 + y_2^2 + (z_2 - r_{SMn})^2}} \right. \\ &\left. + \frac{2(y_2 - y_1)r_{EMn} \sin \alpha + 2(z_2 - z_1)r_{EMn} \cos \alpha}{\sqrt{x_1^2 + (y_1 - r_{EMn} \sin \alpha)^2 + (z_1 - r_{EMn} \cos \alpha)^2} + \sqrt{x_2^2 + (y_2 - r_{EMn} \sin \alpha)^2 + (z_2 - r_{EMn} \cos \alpha)^2}} \right) \\
 &\approx \frac{1}{C} ((y_2 - y_1) \sin \alpha + (z_2 - z_1) \cos \alpha) \end{aligned} \right) \tag{28}
 \end{aligned}$$

where α = Sun-Mars's moons-spacecraft angle.

It can be seen from this equation that the time dispersion width is unrelated to the Mars's moons-to-spacecraft distance. But the time dispersion width is related to the Sun-Mars's moons-spacecraft angle.

This completes the proof of Theorem 2. ■

5. SIMULATION RESULTS. In this section, we study the effect of time dispersion caused by the Mars's moons on the solar TDOA navigation. The simulation conditions are as follows: (1) We use the Mars Pathfinder in the United States as a reference and its initial orbit elements are shown in reference Ning et al. (2016). The simulation time is from 00: 00: 00-000 UTCG on July 1, 1997, to 16: 55: 00-000 UTCG on July 4, 1997, as the approach phase of the American Mars Pathfinder is in this time interval; (2) The Mars mission in 2018 is simulated (Ma et al., 2019). The elements of its initial orbit are shown in Table 1. The orbit epoch time is at 23: 59: 56-000 UTGG on May 15, 2018. The simulation time is from 00: 00: 00-000 UTCG on January 28, 2019, to 02: 37: 30-591 UTCG on February 1, 2019. The orbit data of the Mars Pathfinder and the Mars mission in 2018 are generated by the Systems Tool Kit (STK). In the last experiment, the orbit data are from the Mars mission in 2018. The other data are from the Mars Pathfinder. The three semi-axis lengths

Table 1. Initial orbit elements

Orbit element	Value
Semi-major axis	885,552,000 km
Eccentricity	0.831317
Inclination	21.7902°
Right ascension of the ascending node	353.168
Argument of periapsis	254.541°
True anomaly	346.612°

of Phobos are 13.5 km, 10.7 km and 9.6 km, and the three semi-axis lengths of Deimos are 7.5 km, 6.0 km and 5.5 km.

In this section, we first analyse the time dispersion caused by Phobos and Deimos, and then analyse some factors that affect time dispersion, such as the Mars's moons-to-spacecraft distance, the Sun-Mars's moons-spacecraft angle, the attitude of Mars's moons, the shapes of Mars's moons and the solar flare. Finally, we compare the 3D TDOA model with the point model.

5.1. *Time dispersion caused by Mars's moons.* Since the Mars's moons is not a point, the 3D TDOA model established in this article treats the Mars's moons as an ellipsoid. The Mars's moons include Phobos and Deimos. The difference between the two is that the lengths of the three axes are different. In this subsection, we study the time dispersion caused by Phobos and Deimos, respectively.

Figure 6 shows the time dispersion caused by Phobos at 00: 00: 00-000 UTCG on July 1, 1997. It can be seen from Figure 6 that the time dispersion on Phobos is a sharp peak. The diffusion width of time is 0.063 ms, and the diffusion width of position caused by this is about 19 km. Figure 7 shows the time dispersion caused by Deimos. It can be seen from Figure 7 that this is not consistent with the time dispersion caused by the Phobos. The profile, diffusion width and probability distributions have all changed, which proves that the three-axis lengths of the Mars's moons have a certain effect on the time dispersion. The time diffusion width caused by Deimos is 0.034 ms, and the corresponding diffusion width of position is approximately 10 km. Figure 8 shows the relationship between the TDOA and time, and the relationship between the dispersion width and time, respectively. From Figure 8, we can see that the TDOA and dispersion width both decrease with time. Because the time comes, the spacecraft gets closer to the Mars's moons. The distance between them is getting shorter.

5.2. *Time dispersion width of different points of the Sun.* As the Sun is a huge sphere, the point position at the solar surface causes the time dispersion to change. In this subsection, we study the time dispersion caused by the Mars's moons at different points at the solar surface, and the width of time dispersion caused by the Mars's moons at the point of the Sun.

Figure 9 shows the time dispersion width distribution of different points at the solar surface. From Figure 9, we can see that with the changing of the solar coordinates, the size of the dispersion width is basically unchanged, about 63 us. The error is quite small, as demonstrated in Subsection 4.1. We take a few points of different solar coordinates as $(0, 0, r_{SMn}-R)$, $(0, R, r_{SMn})$, $(R, 0, r_{SMn})$ and $(0, -R, r_{SMn})$, where R is 695,500 km. We take the middle point of the experimental data as the centre time, and take 0.03 ms as a unit for drawing. And time the dispersion profiles of these points are drawn as shown in

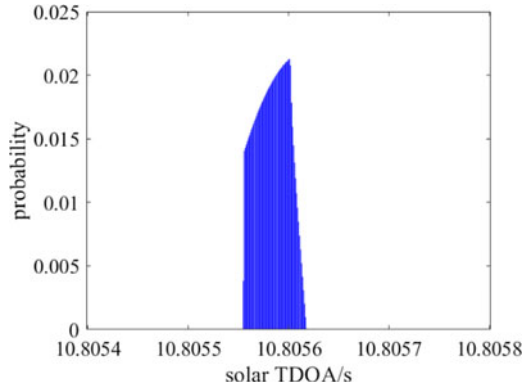


Figure 6. Time dispersion caused by Phobos.

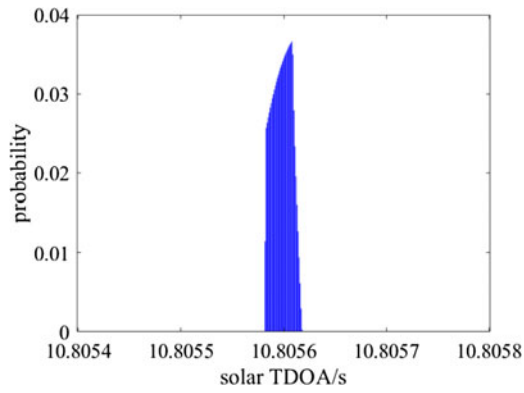


Figure 7. Time dispersion caused by Deimos.

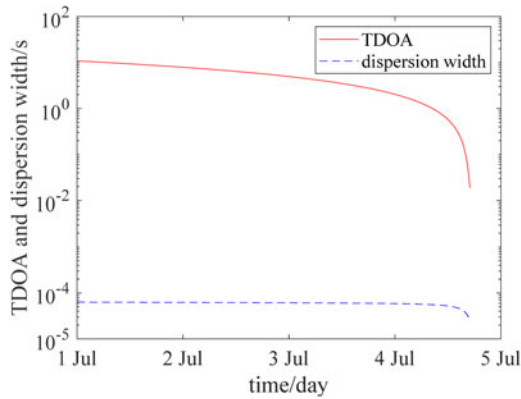


Figure 8. TDOA and dispersion width versus time.

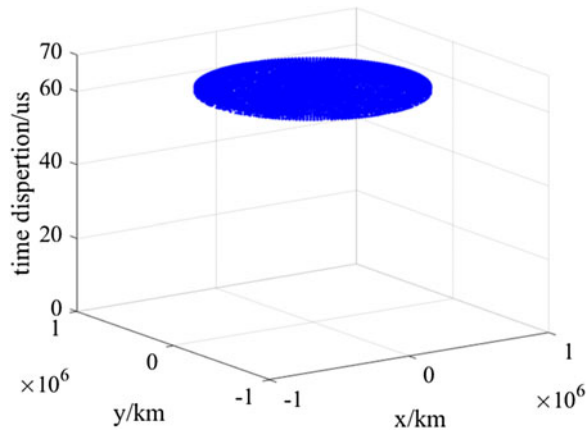


Figure 9. Time dispersion width distribution of Sun.

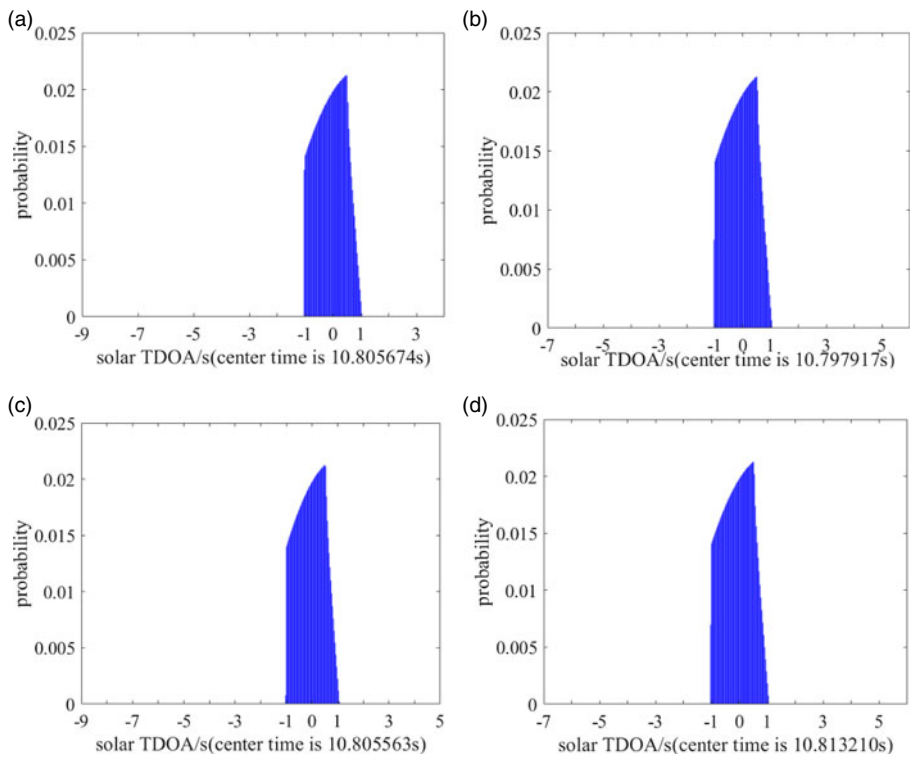


Figure 10. Time dispersion at different points: (a) Sun coordinates are $(0, 0, r_{SMn}-R)$; (b) Sun coordinates are $(0, -R, r_{SMn})$; (c) Sun coordinates are $(R, 0, r_{SMn})$; (d) Sun coordinates are $(0, R, r_{SMn})$.

Figures 10(a)–10(d). We can see that the time dispersion profiles of these points remain almost unchanged, and the time dispersion width is basically the same. The magnitude of the error is 10^{-8} s. The analysis in Subsection 4.1 is being validated.

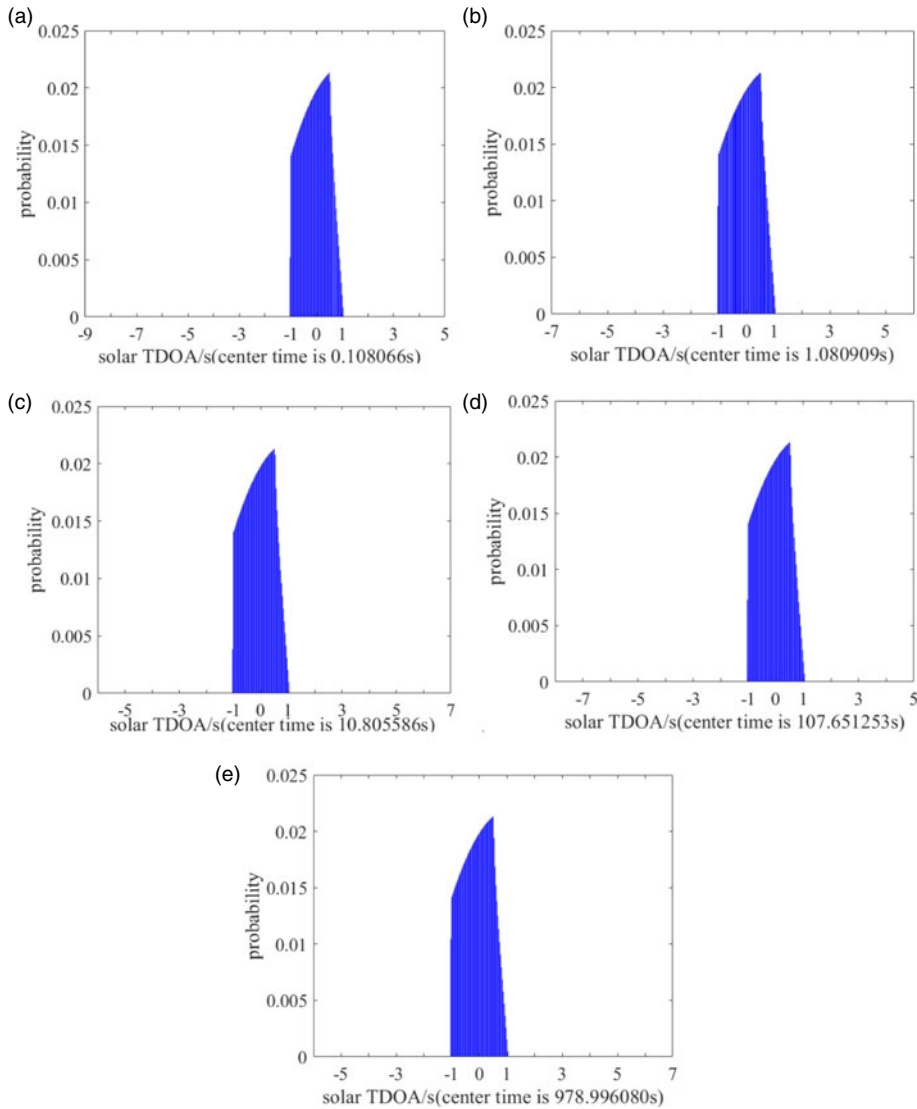


Figure 11. Time dispersion versus the Mars's moons-to-spacecraft distance: (a) Distance is 10^4 km; (b) Distance is 10^5 km; (c) Distance is 10^6 km; (d) Distance is 10^7 km; (e) Distance is 10^8 km.

5.3. Impact of the Mars's moons-to-spacecraft distance. During the approach of the spacecraft to the Mars's moons, the Mars's moons-to-spacecraft distance changes. In this subsection, we study the relationship between time dispersion and the Mars's moons-to-spacecraft distance.

Figures 11(a)–11(e) show the relationship between time dispersion and the Mars's moons-to-spacecraft distance. The Sun-Mars's moons-spacecraft angle is 26.5° . From Figures 11(a)–11(e), we can see that as the Mars's moons-to-spacecraft distance increases, the spread width of the time dispersion, the profile shape and the probability distributions

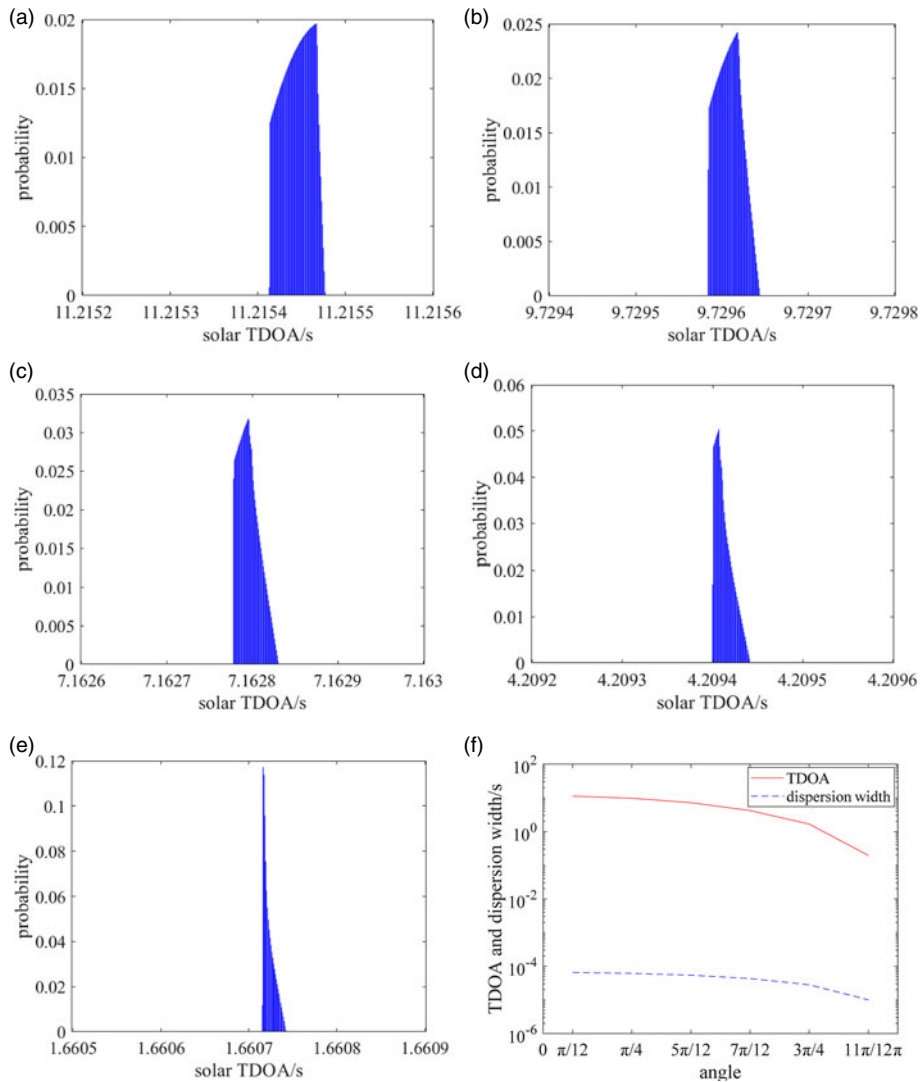


Figure 12. Time dispersion versus the Sun-Mars's moons-spacecraft angle: (a) Angle is $\pi/12$; (b) Angle is $\pi/4$; (c) Angle is $5\pi/12$; (d) Angle is $7\pi/12$; (e) Angle is $3\pi/4$; (f) TDOA and dispersion width versus the angle.

are basically the same, while the TDOA increases. Thus, the time dispersion width is approximately unrelated to the Mars's moons-to-spacecraft distance, as analysed in Subsection 4.2.

5.4. *Impact of the Sun-Mars's moons-spacecraft angle.* During the approach of the spacecraft to the Mars's moons, both the Mars's moons-to-spacecraft distance and the Sun-Mars's moons-spacecraft angle change. In this subsection, we study the relationship between time dispersion and the Sun-Mars's moons-spacecraft angle. The Mars's moons-to-spacecraft distance is $1.712 \cdot 10^6$ km.

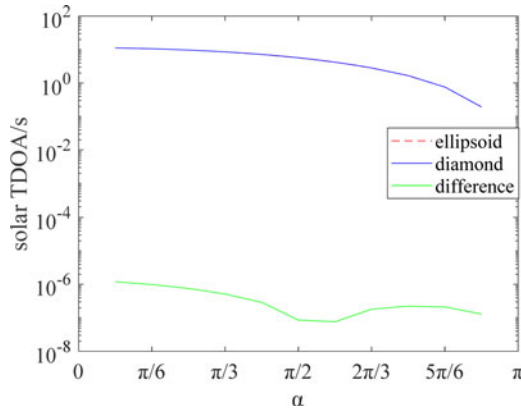


Figure 13. TDOA versus the Sun-Mars's moons-spacecraft angle in different shapes.

Figures 12(a)–12(f) show the relationship between TDOA and the Sun-Mars's moons-spacecraft angle, and the relationship between time dispersion and the Sun-Mars's moons-spacecraft angle. From Figures 12(a)–12(e), we can see that as the Sun-Mars's moons-spacecraft angle increases, the TDOA and the profile shape change, and the time dispersion width decreases. It can be seen from Figure 12(f) that as the Sun-Mars's moons-spacecraft angle increases, the expectation value of the TDOA and dispersion width both decrease with the approximation of a straight line. That is, the Sun-Mars's moons-spacecraft angle is approximately proportional to the solar TDOA and the time dispersion width.

5.5. *Impact of the Sun-Mars's moons-spacecraft angle.* As the spacecraft approaches the Mars's moons, the Sun-Mars's moons-spacecraft angle changes, and this affects the solar TDOA. In this subsection, we study the relationship between the Sun-Mars's moons-spacecraft angle and the solar TDOA under the ellipsoid and the diamond.

Figure 13 shows the relationship between TDOA and the Sun-Mars's moons-spacecraft angle under the ellipsoid and the diamond. As shown in Figure 13, we can see that no matter whether the shapes of the Mars's moons are ellipsoids or diamonds, the solar TDOA decreases as the Sun-Mars's moons-spacecraft angle increases. The values of the TDOA are very close and basically coincide. We can see that the values of the difference curves are quite small, all on the 10^{-6} s order of magnitude and below. And the minimum value is 7.66×10^{-8} s when the Sun-Mars's moons-spacecraft angle is between $\pi/2$ and $2\pi/3$.

5.6. *Influence of Mars's moons attitude.* The three-axes lengths of the Mars's moons are fixed, but the attitude of the Mars's moons cannot be determined. In this subsection, we study the influence of Mars's moons attitude on the time dispersion under the ellipsoid and the diamond.

Figures 14(a)–14(f) show the effect of the attitude of the Mars's moons on the time dispersion when the Mars's moons are ellipsoids or diamonds. It can be seen from Figures 14(a)–14(f) that the time dispersion differs depending on the attitude of the Mars's moons. When the major axis and the minor major axis change, the distribution of the TDOA is different, and both the shapes and the probability distributions change. Table 2 shows the impact of the attitude of Mars's moons on the mathematical expectations of TDOA, which are calculated by weighting. From Table 2, we can see that magnitude of the expectation

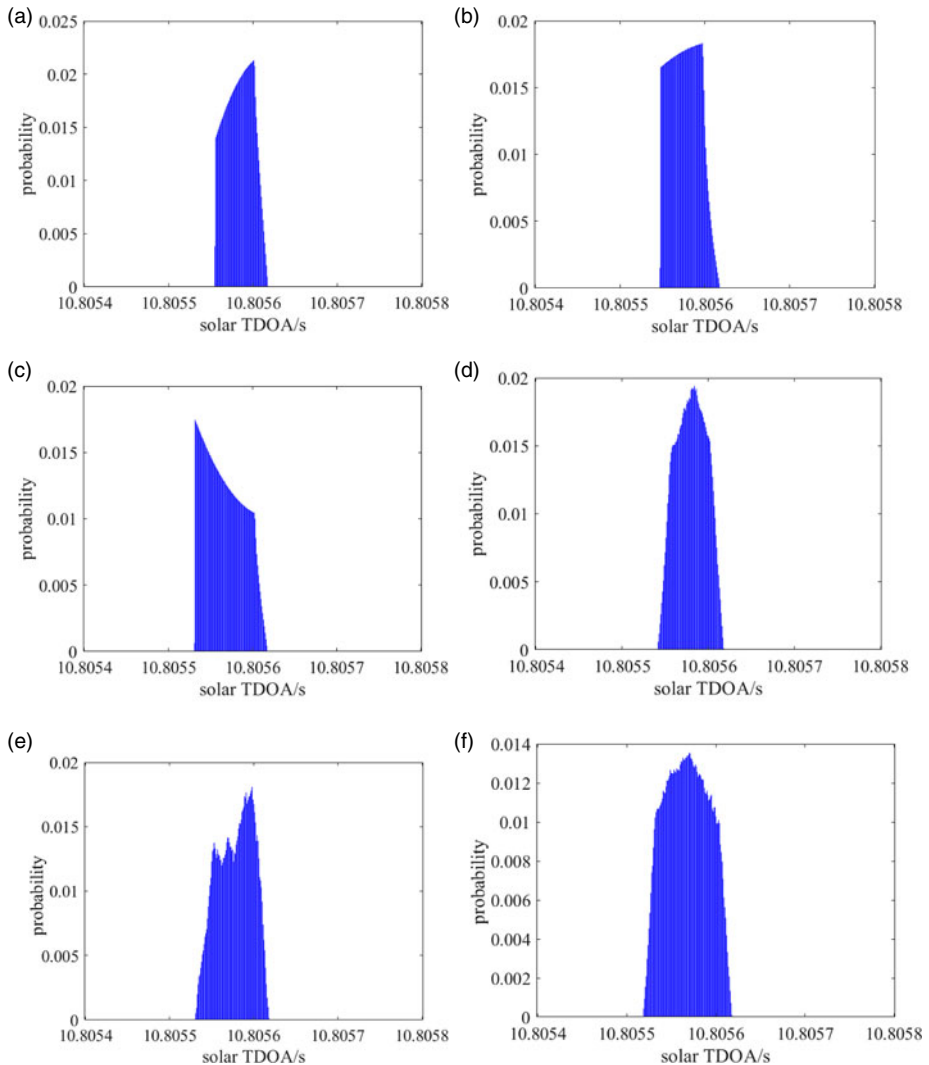


Figure 14. Time dispersion versus Mars's moons attitude: (a) major: x -axis, minor: y -axis (ellipsoid); (b) major: y -axis, minor: z -axis (ellipsoid); (c) major: z -axis, minor: x -axis (ellipsoid); (d) major: x -axis, minor: y -axis (diamond); (e) major: y -axis, minor: z -axis (diamond); (f) major: z -axis, minor: x -axis (diamond).

of the TDOA between the two attitudes is about 10^{-6} s. Therefore, the attitude of Mars's moons has influence on the solar TDOA.

5.7. Influence of the Mars's moons shapes. The actual shape of the Mars's moons are potato shaped. That is, the surface of Mars's moons has depressions, but 3D TDOA model is an ellipsoid with no depressions. In fact, with comparing the potato shape with the ellipsoid, we find that the potato shape is located between the ellipsoid and the diamond. This subsection studies the influence of Mars's moons shapes on the time dispersion.

Figure 15 shows the impact of the Mars's moons shapes on time dispersion. As shown in Figures 15(a)–15(c), the influence of the Mars's moons shapes on the time dispersion

Table 2. Mathematical expectation of TDOA versus attitude

Attitude	Mathematical expectation of TDOA/s
major: x-axis, minor: y-axis (ellipsoid)	10.80558401
major: y-axis, minor: z-axis (ellipsoid)	10.80557652
major: z-axis, minor: x-axis (ellipsoid)	10.80556662
major: x-axis, minor: y-axis (diamond)	10.80558022
major: y-axis, minor: z-axis (diamond)	10.80557776
major: z-axis, minor: x-axis (diamond)	10.80556784

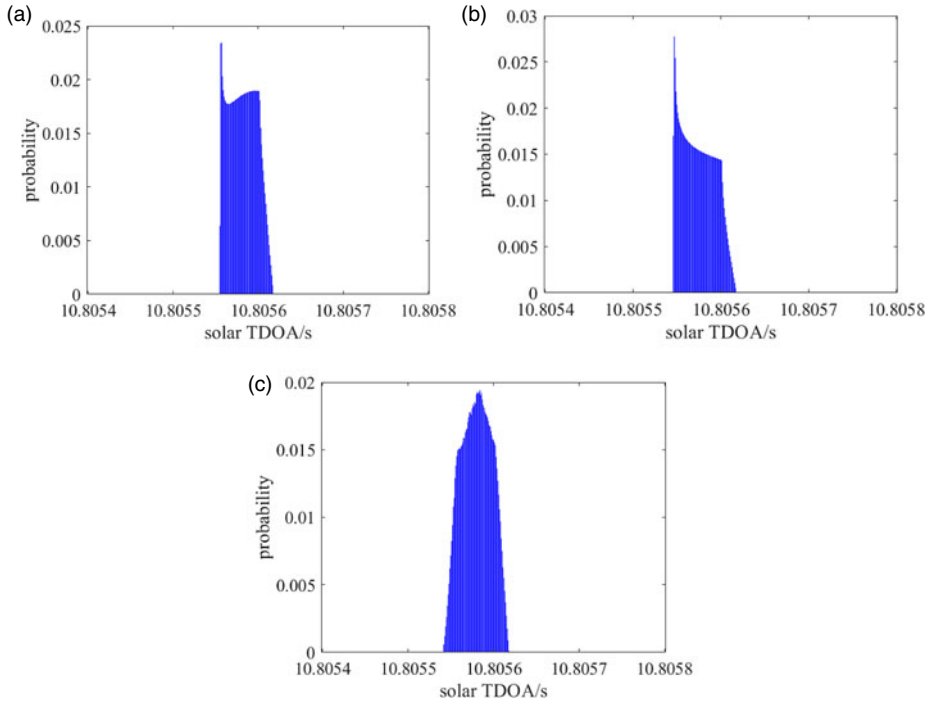


Figure 15. Time dispersion versus Mars's moons shapes: (a) ellipsoid; (b) sphere; (c) diamond.

makes the shapes and probability distributions of the time dispersion in different shapes slightly different. But the diffusion width of the time dispersion and the distribution range in these shapes are the same. And the distribution of the TDOA is different in different shapes, and the distribution is basically smooth. Therefore, we study the expectations of the time dispersion of the three shapes. The difference in expectation of the time dispersion between the ellipsoid and the diamond is 10^{-6} s, which means that the position error is 300 m. Then the difference in expectation of the time dispersion between the potato shape and the ellipsoid model is about 150 m. This error is small for navigation. So, the 3D TDOA model is relatively accurate.

5.8. *Influence of solar flare.* Solar activity is inevitable. So, we must consider its impact when we use sunlight for navigation. In this subsection, we study the influence of solar flare on the time dispersion.

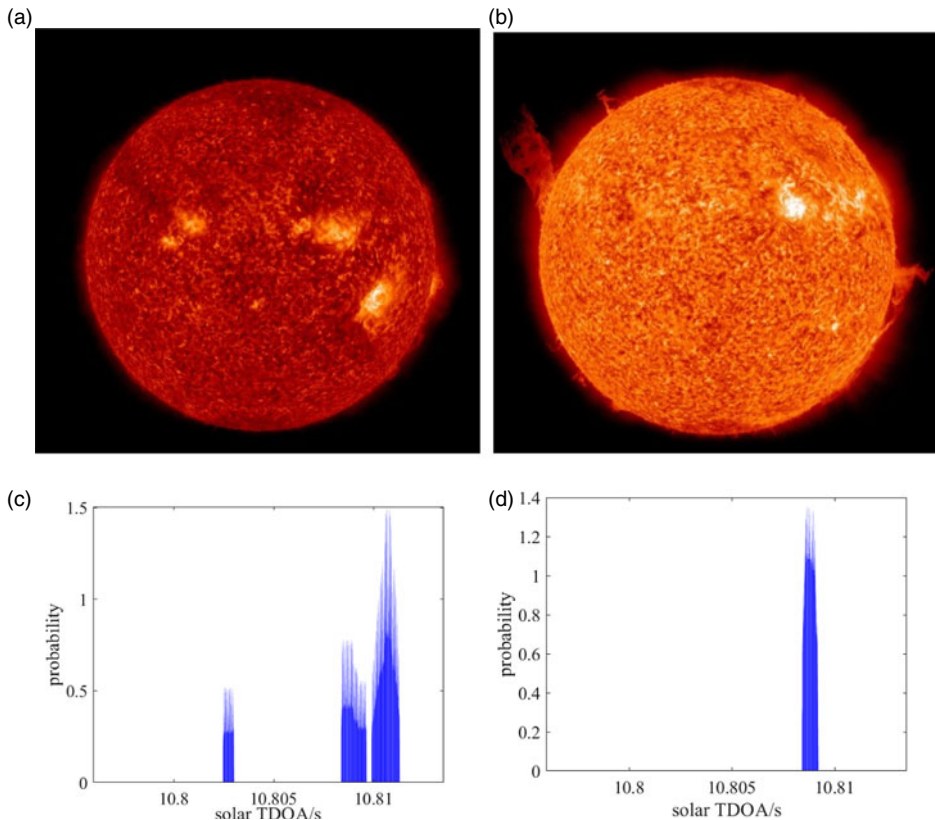


Figure 16. Time dispersion versus solar flare: (a) three flares; (b) one flare; (c) three flares; (d) one flare.

Figures 16(a) and 16(b) are images of the Sun during flare eruption, and Figures 16(c) and 16(d) show the impact of solar flare on the time dispersion. We use these two images for experiments, map the entire image to three-dimensional space and study the time dispersion analysis within a certain threshold. As shown in Figures 16(c) and 16(d), we can see that the solar flare for time dispersion caused by the Mars's moons is influential. The multiple flares on the Sun cause several diffusion segments. The larger the area of a flare on the Sun, is larger the range, and the wider the time dispersion width of the solar TDOA. Besides, the greater the brightness of a flare on the Sun, the greater the probability of the TDOA.

5.9. *Comparison between the 3D model and the point model.* The point model is not accurate, which causes high position error. The 3D TDOA model is more accurate than the point model in both the ellipsoid and diamond. In this subsection, the orbit data of the Mars mission in 2018 is used to study the time dispersions of ellipsoid, diamond and point models.

Figure 17 shows the comparison between the point model and the 3D model, which is under the ellipsoid and the diamond. From Figures 17(a) and 17(b), we can see that the distribution of the time dispersion between the ellipsoid and the diamond is different. But the distribution range is the same, and the distribution is smooth. Table 3 shows the comparison of the time dispersion expectation between the 3D TDOA model and the point model.

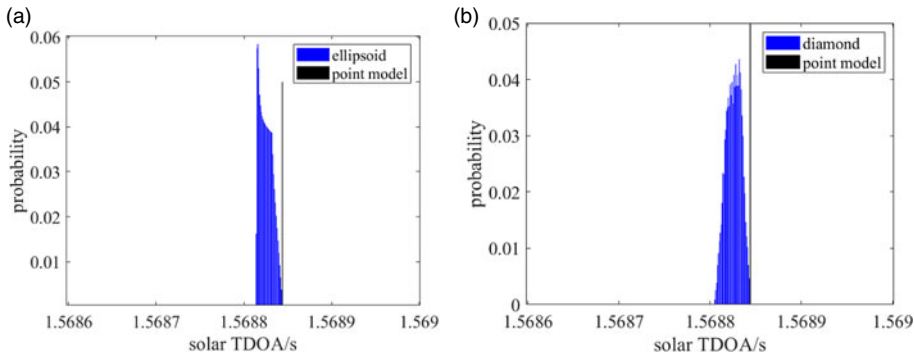


Figure 17. Time dispersion of ellipsoid and diamond: (a) ellipsoid; (b) diamond.

Table 3. Time dispersion expectation of ellipsoid and diamond

Parameter	Value/s
Ellipsoid expectation	1.5688254149
Diamond expectation	1.5688256419
Point model	1.5688443862
Average of ellipsoid and diamond expectation	1.5688255284
Difference between ellipsoid and diamond	2.27×10^{-7}
Difference between point model and mean	1.886×10^{-5}

According to the calculation of the expectation values of the ellipsoid and diamond, we can see from Table 3 that the difference between the two is 2.27×10^{-7} s, which represents a position error of 68 m. This error is negligible, which proves that the 3D TDOA model is accurate. The point model is much different from the expectation value of the ellipsoid or the diamond. If we use the average value of the ellipsoid and the diamond as the standard, then the point model error is 1.89×10^{-5} s, which represents a position error of 5.66 km. Thus, the point model is very inaccurate.

6. CONCLUSION. The Mars's moons model causes time dispersion. The time dispersion of the TDOA caused by the Mars's moons (Phobos and Deimos) has a certain effect on the solar TDOA navigation, which leads to a reduction in navigation accuracy. Therefore, this paper establishes an accurate 3D TDOA model. Theoretical analysis and simulation experiments confirm the properties of time dispersion of the TDOA caused by the Mars's moons.

The 3D TDOA model established in this paper is meaningful as it is reflected in the following aspects: (1) compared with the point model, the 3D TDOA model is more accurate. The point model error is 5.66 km, while the 3D TDOA model error is within 70 m. The simulation results are conducive to the improvement of navigation accuracy; (2) The 3D TDOA model treats the Mars's moons as ellipsoids, and the actual shape of the Mars's moons are potato shaped, which are located between the ellipsoid and the diamond. Simulation results confirm that the accuracy is quite close to the actual situation.

It can be seen from the simulation experiments that the factors that have a large impact on the 3D TDOA model are: (1) the three-axes lengths of the Mars's moons. When the

three-axes lengths change greatly, the time dispersion is greater; (2) the attitude of the Mars's moons. When the major axis and the minor major axis change, the distribution of the TDOA is different, and both the shapes and the probability distributions change; (3) the Sun-Mars's moons-spacecraft angle. As the Sun-Mars's moons-spacecraft angle increases, the TDOA changes, the time dispersion width decreases and the profile shape changes; (4) the flare erupting on the Sun. Flares on the Sun cause several diffusion segments. These factors must be accurately estimated in navigation. The three-axes lengths and attitude data of the Mars's moons are provided by the astronomical database. The solar flare data can be obtained by the onboard CCD. And the Sun-Mars's moons-spacecraft angle can be estimated by the navigation system.

It can be seen from the simulation experiments that the Mars's moons-to-spacecraft distance has little influence on the 3D TDOA model. As the Mars's moons-to-spacecraft distance increases, the spread width of the time dispersion, the profile shape and the probability distribution are basically the same. This factor has little influence on navigation accuracy and do not require accurate estimation.

ACKNOWLEDGEMENTS

This study was supported in part by the National Natural Science Foundation of China (Nos. 61873196, 61772187, and 61501336).

REFERENCES

- Chen, X., Sun, Z. W., Zhang, W. and Xu, J. (2019). A novel autonomous celestial integrated navigation for deep space exploration based on angle and stellar spectra shift velocity measurement. *Sensors*, 19(11), 2555.
- Christian, J. A. (2019). StarNAV: autonomous optical navigation of a spacecraft by the relativistic perturbation of starlight. *Sensors*, 19(19), 4064.
- Fang, J. C., Ning, X. L. and Liu, J. (2017). *Principle and Methods of Spacecraft Celestial Navigation*. 2nd ed. Beijing: National Defense Industry Press. [Chinese].
- Kang, Z. W., Xu, M. X., Liu, J. and Li, N. (2017). Doppler velocity measurement based on double measurement model and its integrated navigation. *Journal of Astronautics*, 38(9), 964–970. [Chinese].
- Konopliv, A. S., Asmar, S. W., Bills, B. G., et al. (2011). The Dawn gravity investigation at Vesta and Ceres. *Space Science Reviews*, 163(1–4), 461–486.
- Li, S., Cui, P. Y. and Cui, H. T. (2006). Autonomous navigation and guidance for landing on asteroids. *Aerospace Science and Technology*, 10(3), 239–247.
- Liu, J., Fang, J. C., Kang, Z. W., et al. (2015a). Novel Algorithm for X-ray Pulsar Navigation Against Doppler Effects. *IEEE Transactions on Aerospace and Electronic Systems*, Vol. 51(1), 228–241.
- Liu, J., Fang, J. C., Yang, Z. H., et al. (2015b). X-ray pulsar/Doppler difference integrated navigation for deep space exploration with unstable solar spectrum. *Aerospace Science and Technology*, 41, 144–150.
- Liu, J., Fang, J. C. and Liu, G. (2017a). Solar frequency shift-based radial velocity difference measurement for formation flight and its integrated navigation. *Journal of Aerospace Engineering*, 30(5), 04017049.
- Liu, J., Fang, J. C., Liu, G. and Wu, J. (2017b). Solar flare TDOA measurement using direct and reflected light for Mars exploration. *IEEE Transactions on Aerospace & Electronic Systems*, 53(5), 2469–2484.
- Liu, J., Ning, X. L., Ma, X., et al. (2019). Geometry error analysis in solar Doppler difference navigation for the capture phase. *IEEE Transactions on Aerospace and Electronic Systems*, 55(5), 2556–2567.
- Liu, J., Li, Y. Y., Ning, X. L., et al. (2020). Modeling and analysis of solar doppler difference bias with arbitrary rotation axis. *Chinese Journal of Aeronautics*. doi:10.106/j.cja.2020.04.034.
- Long, A. C., Leung, D., Folta, D. and Gramling, C. (2000). Autonomous Navigation of High-Earth Satellites Using Celestial Objects and Doppler Measurements. In *Proceeding AIAA/AAS Astrodynamics Specialist Conference*, 1–9.
- Ma, X., Ning, X. L., Chen, X., et al. (2019). Geometric coplanar constraints-aided autonomous celestial navigation for spacecraft in deep space exploration. *IEEE Access*, 7, 112424–112434.

- Ning, Z. J., Li, D. and Dai, Y. (2016). Study for celestial speed detection of integrated navigation in deep space exploration. *Journal of Deep Space Exploration*, 3(3), 225–227. 245.
- Ning, X. L., Gui, M. Z., Zhang, J., et al. (2017). Solar oscillation time delay measurement assisted celestial navigation method. *Acta Astronautica*, 134, 152–158.
- Ning, X. L., Gui, M. Z., Fang, J. C., et al. (2018a). A novel autonomous celestial navigation method using solar oscillation time delay measurement. *IEEE Transactions on Aerospace and Electronic Systems*, 54(3), 1392–1403.
- Ning, X. L., Gui, M. Z., Fang, J. C., et al. (2018b). A novel differential Doppler measurement-aided autonomous celestial navigation method for spacecraft during approach phase. *IEEE Transactions on Aerospace and Electronic Systems*, 53(2), 587–597.
- Pantalone, B. and Kudenov, M. W. (2018). Initial orbit determination using Doppler shift of Fraunhofer lines. *Celestial Mechanics and Dynamical Astronomy*, 130(12), 80.
- Sheikh, S. I., Pines, D. J., Ray, P. S., et al. (2006). Spacecraft navigation using X-ray pulsars. *Journal of Guidance, Control, and Dynamics*, 29(1), 49–63.
- Sun, H. F., Bao, W. M., Fang, H. Y., et al. (2016). Effect of X-ray energy band on the X-ray pulsar based navigation. *Aerospace Science and Technology*, 58, 150–155.
- Wang, D. Y., Huang, X. Y. and Guan, Y. F. (2007). GNC system scheme for lunar soft landing spacecraft. *Advances in Space Research*, 42(2), 379–385.
- Wang, Y. D., Zheng, W. and Zhang, D. P. (2017). X-ray pulsar/starlight Doppler deeply-integrated navigation method. *The Journal of Navigation*, 70(4), 829–846.
- Wang, Z. H., Huang, X. M., Liu, J., et al. (2020). Stellar spectrum-based relative velocimetry with spectrometer and its integrated navigation. *Optik*, 207.
- Yan, J., Zhu, S. Y. and Wang, L. N. (2016). Autonomous Optical Navigation Approach Aided by Radio Beacon for Deep Space Spacecraft. *2016 Chinese Control and Decision Conference (CCDC)*, IEEE, 6354–6359.
- Yu, Z. S., Cui, P. Y. and Zhu, S. Y. (2014). On the observability of Mars entry navigation using radiometric measurements. *Advances in Space Research*, 54(8), 1513–1524.
- Yu, Z. Y., Liu, J., Pan, C., et al. (2019). Solar TDOA measurement and integrated navigation for formation flying. *Proceedings of the Institution of Mechanical Engineers*, 233(12), 4635–4645.
- Zhang, H., Jiao, R. and Xu, L. P. (2019). Formation of a Satellite Navigation System Using X-Ray Pulsars. *Publications of the Astronomical Society of the Pacific*, 131(998), 045002.